IOP Publishing Smart Materials and Structures
Smart Mater. Struct. **23** (2014) 077004 (10pp) doi:10.1088/0964-1726/23/7/077004

Technical Note

Design of a high-lift experiment in water including active flow control

T Beutel[1], S Sattler[2], Y El Sayed[2], M Schwerter[1], M Zander[3], S Büttgenbach[1], M Leester-Schädel[1], R Radespiel[2], M Sinapius[3] and P Wierach[4]

[1] Institute of Microtechnology (IMT), Technische Universität Braunschweig, Alte Salzdahlumer Straße 203, 38124 Braunschweig, Germany
[2] Institute of Fluid Mechanics (ISM), Technische Universität Braunschweig, Hermann-Blenk-Straße 37, 38108 Braunschweig, Germany
[3] Institute for Adaptronics and Functional Integration (IAF), Technische Universität Braunschweig, Langer Kamp 6, 38106 Braunschweig, Germany
[4] Institute of Composite Structures and Adaptive Systems (IFA), Deutsches Zentrum für Luft- und Raumfahrt e.V. (DLR), Lilienthalplatz 7, 38108 Braunschweig, Germany

E-mail: m.sinapius@tu-braunschweig.de

Received 22 July 2013, revised 8 April 2014
Accepted for publication 15 April 2014
Published 21 May 2014

Abstract

This paper describes the structural design of an active flow-control experiment. The aim of the experiment is to investigate the increase in efficiency of an internally blown Coanda flap using unsteady blowing. The system uses tailor-made microelectromechanical (MEMS) pressure sensors to determine the state of the oncoming flow and an actuated lip to regulate the mass flow and velocity of a stream near a wall over the internally blown flap. Sensors and actuators are integrated into a highly loaded system that is extremely compact. The sensors are connected to a bus system that feeds the data into a real-time control system. The piezoelectric actuators using the d_{33} effect at a comparable low voltage of 120 V are integrated into a lip that controls the blowout slot height. The system is designed for closed-loop control that efficiently avoids flow separation on the Coanda flap. The setup is designed for water-tunnel experiments in order to reduce the free-stream velocity and the system's control frequency by a factor of 10 compared with that in air. This paper outlines the function and verification of the system's main components and their development.

Keywords: MEMS pressure and wall shear stress sensor, active flow control, piezoelectric actuator

(Some figures may appear in colour only in the online journal)

1. Introduction

It is general knowledge that the increase in air traffic in the future will lead to additional flights from smaller airports near urban areas. To support public interest and to ensure the quality of urban life, more efficient and quieter high-lift systems will have to be developed. This is essential to meet the demands of tomorrow's mobility and logistics.

One approach to increase high-lift efficiency is the boundary-layer control of airfoils with highly deflected flaps using the Coanda effect. This effect is based on the finding that a thin jet with high momentum will follow a surface, even if the surface is curving away from the jet. For boundary-layer control on an aircraft wing, a small jet of pressurized air, the Coanda jet, is blown tangentially to the surface at the leading edge of the flap. The jet follows the contour and entrains the outer flow that normally would separate from the flap. This

leads to an attached flow over the whole flap and very high lift coefficients at around $c_L = 6$ [10], which permit a steep and therefore quiet takeoff and landing. One disadvantage of this approach is the large mass flow required and hence the high power needed to drive the jet. Recent studies [1] indicate that this leads to engine growth and hence adverse effects on the overall aircraft level. A main topic for research in active high-lift systems is therefore the increase in efficiency of these systems.

One promising way to increase efficiency is to introduce unsteady blowing. Recent numerical and experimental studies [2, 3] show the advantage of unsteady blowing. Periodically exciting the shear layer between the outer flow and the jet increases the mixing and therefore helps to entrain the outer flow with less momentum of the jet. In addition, the inertia keeps the flow attached to a certain extent when the jet is switched off, thus directly saving this mass flow. Although most studies use valves to control the mass flow, the approach proposed herein of boundary-layer control with a highly deflected Coanda flap makes use of an actuated lip that forms a jet nozzle that regulates the mass flow by a variable slot opening. A further increase in efficiency can be expected by introducing closed-loop control of the unsteady blowing. Because flow conditions on an aircraft wing change, for example, by gusts, a system capable of adapting to these changes will be more efficient than a system that runs continuously in one specified state.

Closed-loop active flow control is at present a broad area of research. Geometrically simple test cases such as the cylinder [4, 7] and the bluff body [8] are used to develop and adapt control methods, but flows around airfoils have also been also investigated [5, 6]. Use of the Coanda effect on highly deflected flaps has been investigated for decades (several studies have been done at TU Braunschweig). Detailed numerical analyses of internal blowing on Coanda surfaces, as well as wind-tunnel testing to validate the numerical simulations, have been performed. Two- (2D) and three-dimensional (3D) numerical simulations were used to optimize the geometry of the Coanda flap. The lift gain factor, a measure of system efficiency, could be improved by optimizing slot height, Coanda radius, flap length, and flap angle [17, 18]. The experimental data matched the numerical results well and validated the simulations [19, 20]. Further simulations were conducted with a wing-body combination using the optimized airfoil. Spanwise varying mass flow was simulated to optimize the wing stall behavior [9].

In the approach presented herein, an actuated lip is used to regulate the mass flow and the velocity of a wall near stream over an internally blown flap. This jet flow is used to accelerate the boundary layer so as to keep the flow attached to the strongly deflected Coanda flap. The lip's deformation, shown in figure 1(c), is achieved by piezoceramic actuators embedded in the high-grade steel lip. This actuated lip in combination with a closed-loop controller is expected to deliver high blowing efficiency. A standard controller type such as a proportional-integral-derivative (PID) controller is used in the first experiments to keep the complexity low. The controller parameters will be determined experimentally.

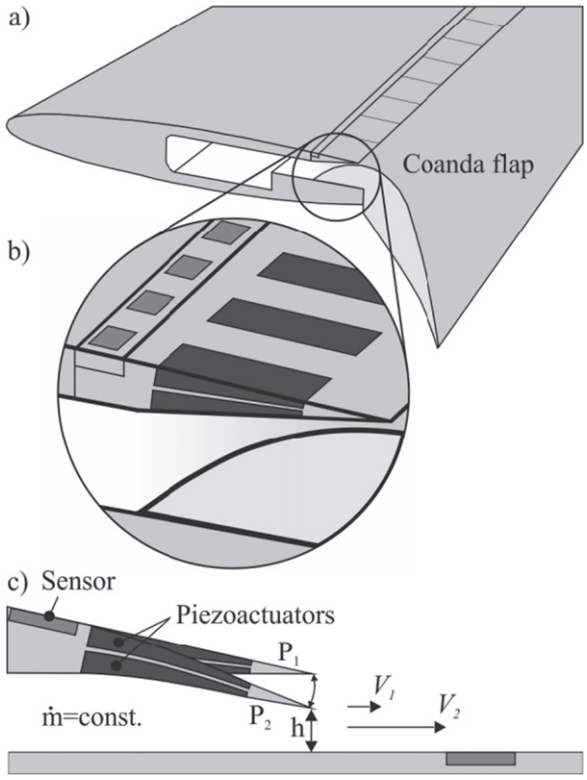

Figure 1. Coanda flap including an actuated lip: (a) overview; (b) detailed view of the actuated lip; (c) cross-sectional view of the simplified principle.

Feedback for the controller is provided by pressure and shear stress on the lip measured by embedded microelectromechanical (MEMS) pressure and wall shear-stress sensor arrays. These sensors are custom made to measure non-intrusively, as shown in figure 1(b). The final goal is to achieve high fluid mechanical efficiency by means of a sensor-actuator system embedded in highly loaded fiber material.

To achieve high efficiency, the mass flow of the fluid has to be reduced and kept to a minimum. This requires continuous measurement of the flow condition at the Coanda flap and a fast reaction by the lip. The tests will be done in a water tunnel within a Reynolds number range of up to 2×10^6. Because the flow velocity in a water tunnel is smaller by a factor of roughly 10 than in air, time-resolved measurements and closed-loop control are much easier.

2. Water-tunnel model with integrated sensors and actuators

The model for the proposed experiment had to be designed based on the requirements of the water tunnel. These include large structural loads; limited space for sensors, actuators, cables, and so on; and watertight connections between all parts. Special care was therefore taken in designing and integrating all the vital components. Model, sensors, and actuators were jointly designed, and thus limitations in one field led to new solutions in others.

2.1. Constraints

Running an experiment in water leads to some constraints that do not exist in a typical wind-tunnel experiment. Cavitation has to be avoided because it can cause damage to the surface of the model. The water tunnel therefore was pressurized to 2 bar compared with ambient pressure.

All connections between the model and the tunnel have to be sealed properly to avoid leakage. Additionally, all electronic parts have to be covered. The hot film used on the flap is treated with a special coating. Although the water tunnel provides similar Reynolds numbers, high mechanical loads on the model have to be considered because of the density of water compared with the density of air (1000 versus 1.225 kg m^{-3}). Assuming a Reynolds number of 1×10^6, the smaller flow velocity of 3.3 m s^{-1} in the water tunnel compared with 50 m s^{-1} in the wind tunnel still leads to an increase in dynamic pressure on the model by a factor of 3.5. With further increases in Reynolds number in the water tunnel, this model load factor increases up to 11.5. Such an increase in load poses challenges for material strength because Young's modulus has to be chosen sufficiently large to avoid unacceptable model deflections.

Another point to be considered is the static pressure inside the model. In a wind tunnel, the mass flow for the Coanda wall jet is generated by a high-volume, low-pressure compressor. Hence the static pressure inside a typical wind tunnel model is approximately 0.2 bar larger than the static tunnel pressure. In water experiments, the mass flow for the jet in the water tunnel is provided by a 15 kW high-pressure pump. Water is extracted from the tunnel circuit and fed into the model from both sides. Using the momentum similarity of the wall jet, the static pressure inside the model is approximately 6 bar larger than the outer pressure in the tunnel. This leads to large loads, especially for the bolts connecting the major model parts.

Usually the material used for wind-tunnel models is fiber composite or aluminum alloy. Because the model is meant to stay in the water tunnel for extended experimentation periods, corrosion prevention is an important aspect and not covered by these materials. Here corrosion prevention is achieved by the choice of stainless steel as the appropriate material for the model. Figure 2 shows the main parts of the water-tunnel model without instrumentation. One can see the massive intake, which also functions as the connection to the tunnel sidewalls. All bolted connections are accessible from the lower side of the model so as not to disturb the much more sensitive upper model surface.

2.2. Airfoil

The Coanda effect on airfoils with highly deflected flaps has been investigated at the Institute of Fluid Mechanics for years using the well-known reference airfoil DLR F-15 [21]. The sensitivities and optimal geometries for Coanda radius, slot height, and so on have been found and tested numerically [17, 18] and in wind-tunnel experiments [19, 20]. Recent numerical studies have shown further increases in efficiency

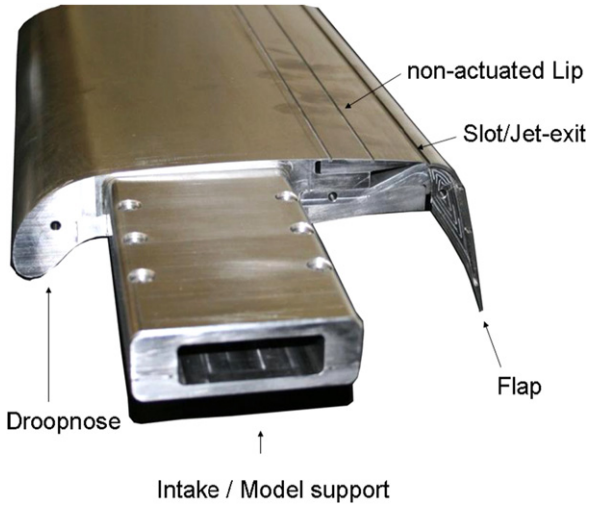

Figure 2. Side view of the model with mounted dummy lip.

by adding a flexible droop nose [10]. The advantages of the droop-nose configuration are improved stall behavior, reduction of the necessary mass flow by almost 30%, and reduction of pitching moment by 15%. This new geometry therefore has been chosen for the water-tunnel model. The model has a span of 1000 mm and a chord length of 300 mm. This allows a Reynolds number of about 2×10^6 the be achieved and therefore eases problems with transition fixing at the airfoil leading edge. The aspect ratio of the model will allow for quasi-2D flow based on previous experience [21].

2.3. Design of the model

The model is made of upper and lower wing boxes, flap, and lip, as shown in figure 2. Both wing boxes form two channels on each side where the water supply for the Coanda jet is connected. This intake also functions as the connection to the tunnel sidewalls. The water is routed inside the model to the slot between the flap and the lip, where it exits the model. As mentioned earlier, the loads on the water-tunnel model are far larger than those on a comparable wind-tunnel model. The preliminary design is based on simple analytical methods, whereas finite-element (FE) modeling is used for detailed analysis of stress and strain. The analysis shows that the major design challenge is at the connection between the upper and lower wing boxes. Because stainless bolts are not available in high-property classes, large bolt diameters have to be used. Similarly difficult is the transmission of shear forces. Here a form-locking tooth system for the front connection and fitting bolts for the rear connection are selected as a suitable solution. All bolted connections are accessible from the lower side of the model so as not to disturb the much more sensitive upper model surface. To compensate for machining tolerances, the slot height for the Coanda jet must be adjustable. The solution found for the model uses spaced bolts to bend the flap locally up or down, changing the gap accordingly. This forced bending locally leads to additional stresses. FE simulations therefore were conducted to quantify the loads and to predict the resulting change in gap height under load.

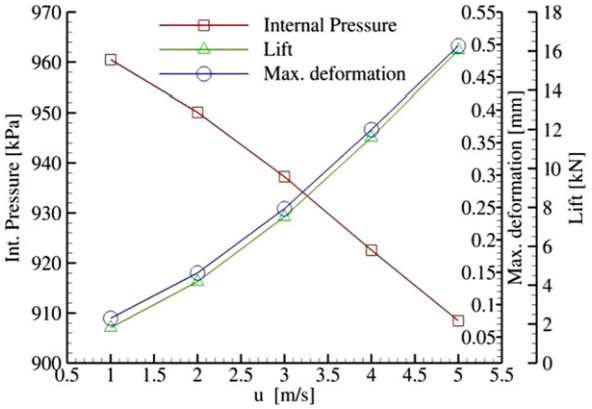

Figure 3. Effect of free-stream velocity on the lift on the model, the pressure of the Coanda jet supply, and the maximum deformation of the model.

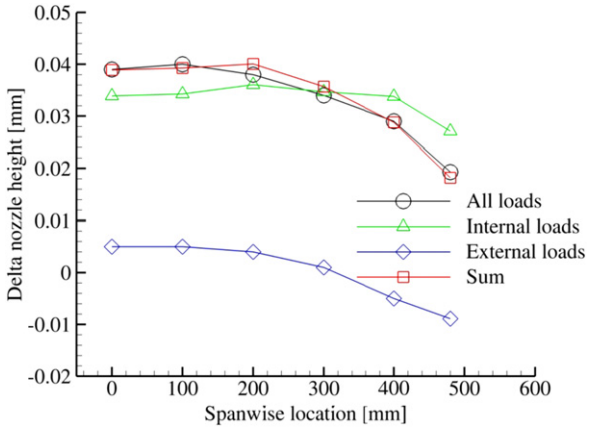

Figure 4. Change in Coanda nozzle exit height over the span of the model under internal, external, and combined loading conditions and the sum of the internal and external loading conditions.

The loads to which the model is subjected can be divided into internal and external loads. The internal loads are caused by the high-pressure water supply needed for the Coanda jet flowing through the model, whereas the external loads are the result of induced hydrodynamic forces acting on the model. The hydrodynamic and internal pressure loads at the various free stream velocities were obtained via numerical simulation. These simulations yield the change in lift and internal loads relative to the free stream velocity, as shown in figure 3.

Whereas the external loads are directly proportional to the square of the free-stream velocity, the internal loads decrease with the free-stream velocity: This is caused by the drop in static pressure outside the Coanda nozzle as the free-stream velocity increases. Therefore, a smaller internal pressure is needed to keep up the pressure difference over the wall jet nozzle. Figure 3 shows the maximum model deformation calculated by FE simulations at the lip position in the midsection of the model at those velocities. The deformation follows the trend of the lift curve, indicating that the external loads are dominant.

To ensure quasi-2D flow, the Coanda nozzle dimensions have to be as even as possible along the span of the model under load. To determine the influence of model bending on nozzle height, FE simulations were done with each type of load separately.

Figure 4 shows the change in nozzle height with the dummy lip at the target flow conditions along the half-span of the model, with the zero position corresponding to the midsection of the model. It can be seen that the nozzle height increases by about 20% at the midsection and by about 10% at the edges under the combined loads. Whereas the internal forces cause most of the change in nozzle exit height, this change is fairly constant over the span. External forces, on the other hand, have only a minor effect on the nozzle exit height and an even lesser effect over the span. Also seen in the figure is the sum of the changes in nozzle exit height with each type of load. This sum follows the values obtained with the combined loads, thereby validating all load cases.

To finally validate the FE simulations, load tests are needed. Because such tests are difficult to carry out given the complicated loading conditions on the model, not to mention the risk of damaging the model, it was decided to do load testing in a water tunnel. By increasing the free-stream velocity under constant blowing conditions, the load on the model will be increased gradually while the deformation in the model is measured optically and checked against the FE simulations under similar loading conditions.

2.4. Sensor integration/electrical insulation

The model is equipped with 68 pressure taps to measure the steady pressure distribution in the midsection. The taps are not distributed evenly but are adjusted to the calculated pressure distribution. Therefore, only a few taps are located on the lower side, and more are located at the nose and the jet exit to resolve the suction peaks and the stagnation point. The tubes are routed inside the model and exit through a sealed interface in the tunnel sidewall. Because measurements of the pressure fluctuations on the flap are required as well, four additional pressure taps on the flap are provided in a second section. The taps have the same coordinates in chord direction as the taps on the main pressure-measuring section to allow for better comparison. Because of a shortage of space, built-in sensors were not seen as an option, so external transducers were installed next to the sidewall instead. The cutoff frequency of the tubes is 10 times larger than the highest frequency to be measured because the damping in water-filled tubes is far smaller than that in air. Additionally, a hot-film array with 20 elements was applied on the flap to measure time-resolved shear stress and frequency spectra of the flow. The array is equipped with a waterproof coating.

Integration of the actuated lip includes the routing of all cable lines. Because the space for cables is limited for structural reasons, the sensor elements in the lip are connected by a bus system, reducing the wiring effort substantially. The groove for the sensor elements is located in the least-loaded part of the lip, as shown in figure 5. A second groove is provided in the upper wing box to embed the wiring for the actuator power supply, which is only partly routed inside the lip.

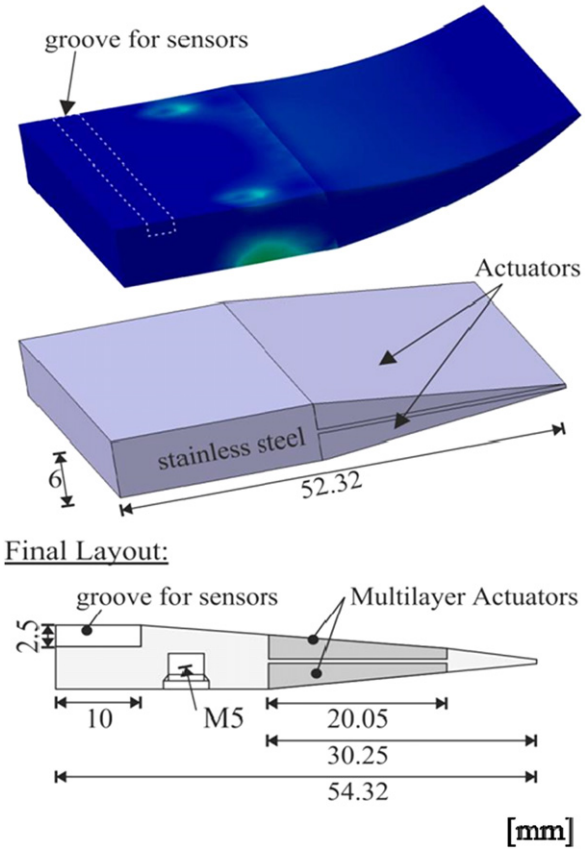

Figure 5. Preliminary FE analysis of the lip to locate the position of the sensor groove and final layout of the actuated lip (dimensions in millimeters).

3. Design of microfabricated sensors

In the experiments, the wall shear stresses and pressure have to be measured because they will be used for closed-loop control. Both the pressure at the location upstream of the lip and the shear stress change significantly with a changing flow state, for example, beginning flow separation or moving of the stagnation point, which have been shown in previous simulations [10]. For these flow quantities, many measurement approaches are possible. In particular, the pressure measurement has been achieved by a number of different approaches, such as piezoresistive, piezoelectric, inductive, resonance, and capacitive. Most of them also have been done at micrometer scale using a wide range of technologies [15].

For measurement of wall shear stress, a number of different sensor were popular in the past. Some of them have are recent arrivals using silicon bulk micromachining and other technologies, such as thin-film sensors on flexible polyimide foil. For a first attempt, these sensors will be fabricated on different substrates. The pressure sensors will be made of traditional silicon, enabling high accuracy in a noncurved area (see figure 5). The wall shear-stress sensors will be placed on flexible substrate because they are located on a curved surface on the Coanda flap. Further miniaturization is not desired, but an improvement in the reliability and robustness is necessary for this application.

3.1. Requirements

For both pressure and shear-stress measurements, it is essential to nonintrusively detect the state of the flow. In practice, no sensor elements are allowed in the fluid. Therefore, all sensor elements have to be embedded flush to the surface. This reduces the high number of measurement approaches to a few. Additionally, the application in water reduces the options significantly because of the high mechanical loads to which the sensors are exposed. The main advantage of lower flow velocity at the same Reynolds numbers compared with air is just a relevant fact for the control duty cycles. Most of the microfabricated sensors enable very high sampling rates because of their small dimensions. Their low mass leads to high eigenfrequencies just like the low thermal mass in other measurement devices. However, the water itself is expected to be problematic because it causes oxidation and changes of the electrical material properties as a result of water absorption.

As the third and last boundary condition, the embedding process into fiber material has to be mentioned. As described in this paper, the mechanical and thermal loads are relatively high, in practice, in the region of the desired measurement range. Hence the sensors have to be robust enough to withstand these loads without any harm.

3.2. Measurement principles

Pressure measurements can be performed by many different approaches. Piezoresistive elements on a membrane are adequate for this application to achieve high resolution and to be able to easily simulate sensor behavior. The membrane is wet etched in KOH; a reference pressure chamber is created by anodic bonding of a glass cap on the sensor's back. Electrical contact is made by means of through-silicon vias so as to achieve a flat surface. These sensors are specifically tailored for this application. For design and manufacture, significant experience via FE analysis in silicon wet etching and diffusion have been achieved. Details about the processing and testing can be found in Beutel *et al* [12]. In terms of the necessary resolution and measuring frequency, capacitive sensors also would be suitable. As described later, the number of microcontrollers featuring voltage measurements (ADC) is higher than those performing capacitance measurements (CDC). This will be a valuable advantage for the small packaging within the airfoil.

To determine the existing flow conditions, wall shear-stress sensors have to be placed close to the pressure-sensitive element (single sensor) as well as on the Coanda flap (sensor array). Hot-wire sensors are a commonly used technique that is also commercially available (Dantec Dynamic A/S or Tao Systems, Inc.). The measurement concept is based on the phenomenon of convective heat transfer. The electrical power dissipated by a resistor, which is the sensor element, is equal to the heat loss into the fluid. Because of the intrusiveness of this measurement approach and the fragility of the sensor wires, a special form of this principle is preferred, namely, hot-film anemometry. In this case, a thin film replaces the hot wire, leading to higher heat conduction into the substrate that is not negligible in contrast to the losses caused by radiation.

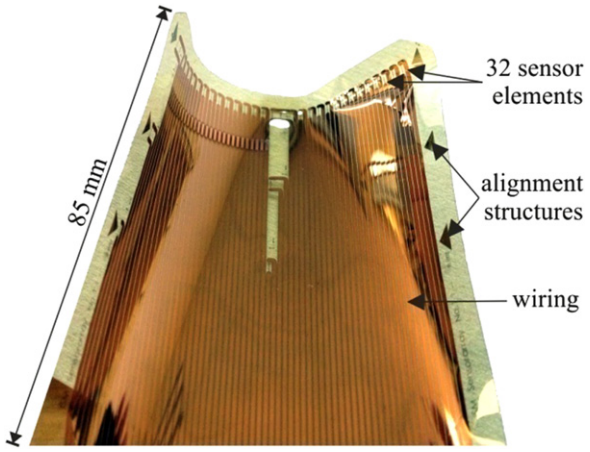

Figure 6. Flexible hot-film sensor array with 32 sensing elements that is suitable to be placed on the curved Coanda flap.

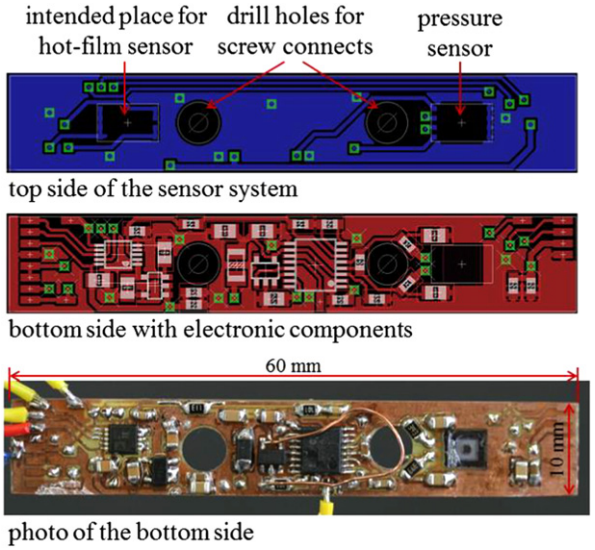

Figure 7. Computer-aided design (CAD) drawings (*above* and *center*) and a photograph (*below*) of the PCB including all relevant electrical components. The pressure sensor is already included; the hot-film sensor will be mounted later at the marked position.

Whereas solid hot-film sensors on a silicon substrate can be used next to pressure sensors, a flexible foil sensor is used on the curved Coanda flap. The sensor's substrate is fabricated using liquid spin-on polyimide, enabling a sensor thickness of down to 7 μm. The hot-film elements are made of nickel because of its high-temperature coefficient of resistance [13]. Figure 6 shows a fabricated hot-film sensor array on 20 μm-thick polyimide foil.

For both types of sensors, detailed manufacturing processes have been developed. This also includes the water reliability, which is necessary for water-tunnel experiments. In tests with spun-on polyimide for covering the hot-film sensor array, only 2 of 20 sensors were damaged after two months of operation in water, even though the sensors were heated frequently [13]. The polyimide covering, combined with an additional diffusion-barrier layer, will be used for both sensors.

In the first attempt, both sensors where designed on separate chips. In the future, the hot-film sensor will be mounted onto the pressure sensor system as well to achieve space-resolved information. This is a substantial step in packaging, and it will be tested and proven in the near future. It is assumed that the hot film influences the piezoresistive pressure measurement. The effect is considered to be small because of the high thermal conductivity of silicon. All four resistors (forming a Wheatstone bridge) are therefore exposed to the same heat, leading to a compensation of temperature effects. This will be proved in the practical experiments.

3.3. Geometry issues

As shown in figure 5, a tiny slot reserved for flow measurement is placed against the stream before the actuated lip and its anchorage. Therefore, the area is not loaded with significant stresses. The microfabricated sensors and signal-conditioning and routing materials have to be placed in the slot, which has sectional dimensions of $10 \times 2.5\,\mathrm{mm}^2$. Although significant improvements in the fields of microelectronics and packaging have been made, the compact mounting of the sensors on a printed circuit board (PCB) is a tough task.

As mentioned earlier, the sensor surfaces have to be flush to the wall. This also applies to the electrical connections. The widely used wire bonding on the top surface is not feasible; in contrast, through-silicon vias (TSV) including flip-chip or ball-grid array (BGA) soldering technique are applicable. The flush sensor concept is intended to be embeddable in fiber materials because fiber is the preferable material for modern aircraft components [12].

In order to avoid tubes to every single sensor, an absolute pressure measurement is preferred. This leads to a design that includes a cavity containing a gas at constant/fixed pressure or vacuum.

Figure 7 shows the PCB design, including analog-to-digital (A/D) electronics for the pressure sensor and the pressure sensor and the intended position of the hot-film sensor. Whereas the hot-film sensor will be controlled and read by an external bridge circuit, the pressure sensor output voltage is directly amplified and digitalized with 3000 samples per second in 16 bit resolution. The boards are designed to connect in series to achieve a flexible adjustment to the measurement environment as well as a reduction in wiring.

Limitations result from the high data rate from each sensor. The smallspace in the model does not allow for the inclusion of any additional wires, and the high-voltage actuators right next to the sensors makes digitalization close to the sensor indispensable.

4. Design and dimensioning of an actively actuated slot lip

Because the design is led by the requirements and constraints defined by the project goals, as stated in sections 1 and 2, several specifications are assumed as given parameters. One

involves the use of advanced multilayer piezoelectric actuators and the d_{33} effect at a low operating voltage of approximately 120 V with high free-strain rates compared with common macrofiber composite (MFC) actuators at this voltage level, as investigated at the DLR by Wierach [14]. Because of the small build envelope in the normal and longitudinal planes in the model for water-tunnel tests, a compact bending actuator configuration was chosen to provide a slot opening of 0.2 mm. The slot has to be opened and closed in static, quasi-static, and dynamic modes with an oscillating slot-lip tip at a maximum of 30 Hz. Because they encounter high loads as a result of the difference between the static pressure inside the model and the pressure in the water tunnel of approximately 6 bar, the slot-lip design and material are pushed into tight tolerance limits. The following sections describe the material and design choices.

4.1. Advanced actuator material

As mentioned earlier, the slot lip is actuated by multilayer piezoelectric actuators using the d_{33} effect. These actuators are standard P-888.30 PICMA Multilayer Piezo Stack Actuators from PI Ceramic (Lederhosen, Germany). The manufacturer states that these standard multilayer piezo actuators have a superior lifetime even under extreme conditions, a very large operating temperature range from −40 to 150 °C, high humidity resistance, excellent temperature stability, high stiffness, peak currents up to 20 A, ultrahigh voltage (UHV) compatibility of up to 10^{-9} hPa, submillisecond response at subnanometer resolution, and an excellent capability of dynamic operation [11]. The low operating voltage of about −20 to 120 V at a high free strain of approximately 1400 μm m^{-1} predestines these actuators for mobile applications. In fact, compared with MFC actuators, multilayer piezoelectric actuators use a 10-times lower operating voltage at the same free strain [14].

Multilayer piezoelectric actuators are also called multilayer composite actuators because of their composition from different materials. They are built up of 60 μm piezoceramic layers and alternating interdigital electrode layers, and the electrodes make contact via an elastic collector electrode. The multilayer composite actuators are built up of multilayer stacks that are diced into plates and embedded in a polymer afterwards. By embedding the plates into a polymer, the piezoceramic material is provided with mechanical stability and electrical insulation and is characterized by easy handling.

Actuator failure that is not the result of fabrication problems is often caused by a short circuit from corrosion and electrical erosion, as climatic exposure tests in water have shown for actuators encapsulated in polymer. Given the ability of the presently used standard multilayer stack actuators to withstand humidity, as described in the PI Ceramic company literature [11], the encapsulation is not yet suitable for a warm-water environment such as that present in the planned water-tunnel tests. Inhibiting water absorption, particularly diffusion, is essential and challenging and therefore an important development approach for actuators used in water tunnels.

4.2. Slot-lip design: requirements and concept dimensioning

The actuating slot lip is built as a trimorphic bending actuator. Trapezoidal multilayer piezoceramic actuators made up of multilayer stacks are able to deflect the tip of the slot lip upward and downward. FE analysis shows the advantage of providing a larger overall slot opening over monomorphic configurations. Moreover, the ability to actuate the tip of the slot lip in both directions at all designated pressure levels promised to be the most desirable characteristic that enables necessary adjustments or even compensation for manufacturing imperfections or undesired deviations once the slot lip is mounted on the water-tunnel model for testing. The slot lip itself is composed of several span-wise segments adding up to approximately 1 m and is later mounted on the water-tunnel model (see figures 1 and 2). Each segment consists of a stainless steel substrate used to build up the backbone of the slot-lip structure and several trapezoidal cut multilayer actuators glued on each side of the metal substrate. This is shown in figure 5, where the slot lip, in this case one segment, is displayed as an FE model and in cross-sectional view showing the current envelope and its major dimensions, as well as the main components such as metal substrate and actuators. The number of slot-lip segments, and therefore the number of separately controllable slot-lip digits, is defined by the water-tunnel model, for example, partitioning of screw holes, acceptable number of wires, and demand for active flow control. For this reason, the number of trapezoidal actuators can vary and is not set yet.

4.3. Design verification and validation with FE analysis and functional bending tests

A functional demonstrator of the actuated slot lip for testing purposes has been built to characterize this assembly in terms of free elongation (in this case, tip deflection), blocking force, and dynamic behavior at the required frequencies. In contrast to a slot-lip segment for the later water-tunnel model, the functional demonstrator offers a larger and flatter interface section with a tap for defined positioning for clamping reasons. The section of the functional demonstrator that holds the actuators exactly matches the dimensions of the slot lip for the water-tunnel model. Another difference lies in the wiring for the control system. The circuit boards with the sensors are not yet embedded in the slot lip in order to keep the demonstrator simple. Figure 8 shows the functional demonstrator, the later-applied sensors, and a one-euro coin as a size comparison. An FE simulation of the 20.54 mm-wide functional demonstrator verifies functional actuation and the applied line load considered as a blocking force

Moreover, the model is able to translate the applied line load into the pressure load occurring later in the water tunnel, given that the experimental realization of a distributed pressure load simulating water pressure is hardly possible. Therefore, a line load that is easily applicable in a standard material testing machine is considered to be sufficient for investigation of the blocking force. The tests can be divided into two stages of complexity for the functional demonstrator.

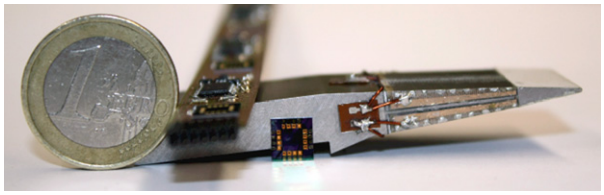

Figure 8. Functional demonstrator and sensors in comparison with a one-euro coin.

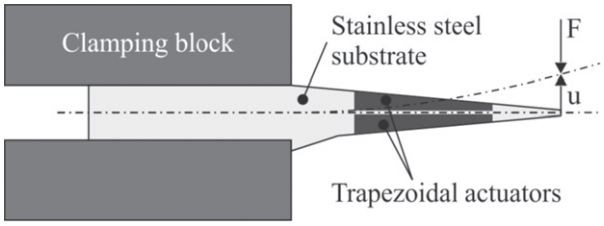

Figure 9. Test setup for measuring the blocking force and tip deflection of the functional demonstrator.

The first stage consists of a simple design in which two trapezoidal cut stack actuators are arranged on each side of a 0.5 mm stainless steel band (not shown). Its cross-sectional design resembles the design of the actuated slot lip, whereas this simple functional demonstrator is only as wide as one stack actuator (~10 mm). The second stage consists of a more complex bending actuator, which leads to a more realistic functional demonstrator (figure 8) with the exact cross-sectional geometry of the slot lip. The functional demonstrator holds four stack actuators on each side. On both functional demonstrators, the tip deflection is measured with a laser triangulator at maximum actuation, that is, at a maximum voltage of 120 V, in a quasi-static mode at 0.1 Hz and in a dynamic mode at 30 Hz while no external load is applied. The layout of the test stand for the complex functional demonstrator is shown in figure 9. The figure shows the two clamping blocks holding the fixed functional demonstrator consisting of the metal substrate and the embedded trapezoidal actuators.

The tip deflection u is measured with a laser triangulator in upward and downward positions versus the nondeflected or neutral (zero) position. This is done with the tip actuator in two operational modes, that is, quasi-static and dynamic. The overall potential tip deflection shown in figure 10 is the sum of the upward and downward absolute values.

The blocking force F was measured In the same test stand. Blocking force is the force when the tip of the slot lip is in the neutral (zero) position at the maximum actuation of the functional demonstrator (120 V). For both stages in quasi-static and dynamic modes, the experimental results show 26% lower average values than the FE results [16], but these values are acceptable and still above the required value of 0.2 mm. For the second stage of development, the test setup for the complex functional demonstrator measures the blocking force as well as the tip deflection with a Zwick BZ005/TN2A material testing machine The tip deflection is measured with a laser triangulator with the slot lip in a quasi-static mode. The

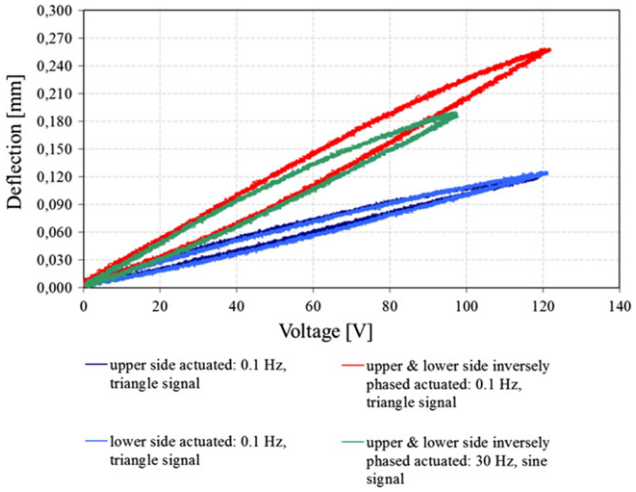

Figure 10. Experimental actuation of the slot lip in different operational modes. Reproduced with permission from [16].

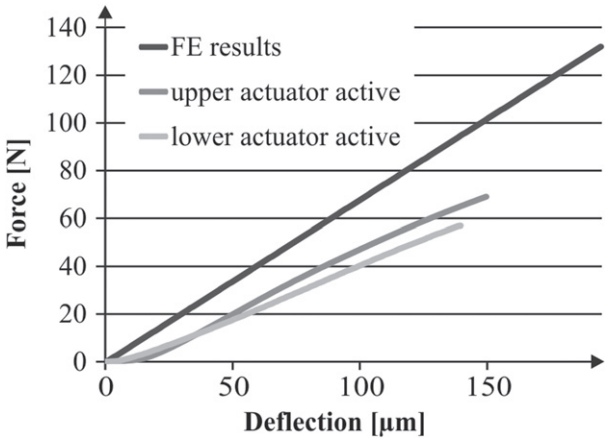

Figure 11. Comparison of blocking force in simulation and experiments. Reproduced with permission from [16].

external load is applied with an anvil on the cross-head of the material testing machine as a line load, and the line load is used to best simulate the pressure that exists in the water-tunnel experiments. These experiments brought unexpected results. The blocking force was only 50% of the value calculated in the FE model. This discrepancy can be explained by the results of a modified FE model, which showed this effect when uncoupling the elements directly at the boundary between the two materials of stack actuator and metal substrate.

As figure 11 shows, in reality, the actuator system creates a much lower blocking force and smaller deflections. The FE results imply that, in reality, the bonding between the stack actuator and the metal substrate is somewhere in between coupled (infinitive stiff) and uncoupled (infinitive soft). Additional investigation under a microscope revealed a glue layer thickness that is at most 10 times that of the calculated layer and the expected thickness from the manufacturing process. In addition, the glue layer is not homogeneously thick along the length of functional demonstrator.

4.4. Challenges for the actuator concept

Current challenges for the actuated slot lip involve several different areas of interest. One is that the results of bending tests measuring blocking forces did not resemble the ideal FE results. The FE model does not take the influence of the glue layers and, most important, their thickness into account. This has to be considered in a more detailed and refined FE model of the functional demonstrator. The current FE model is partially validated, however, by the results of the experiments measuring tip deflection performed with a line load. This serves as the basis for further developments and complete validation. A completely validated FE model then would enable comprehensive numerical studies with the pressure load as it is found in the water tunnel. Furthermore, the functional demonstrator itself needs to be refined regarding its manufacturing accuracy. In particular, the FE model emphasizes that the effect of a thinner and more homogeneous glue layer must be addressed to reach higher geometric accuracy. In addition, the strategy of considering different and modified glues or different mechanical solutions could decrease the problem of a soft bonding layer. Another challenge is the water environment of the water tunnel. This environment is highly undesirable for all electrical devices, especially the piezoceramic actuators, which have only a thin resin coating. Direct contact with water or diffusion of water into the actuator can cause electrolysis and oxidation, leading to flashovers or short circuits, thus reducing actuation or causing total failure. To investigate these effects, experiments were conducted with standard d_{33} Patch multilayer piezocomposite actuators (using the same basic materials and layout as the ones employed in the functional demonstrator) without any additional coating except the mechanical stabilization layers made of Kapton foil and resin. Two test setups were arranged, one in a water bath at room temperature and another in a climate chamber at 70 °C and a relative humidity of 85%. After storing the specimens in these environments for up to 8 weeks, the specimens were actuated with a triangular-function electrical impulse at 0.1 Hz while measuring the elongation and recording the typical hysteresis curve. For the specimens in the water environment, short circuits occurred after 1 day of storage, and the actuators functioned properly only for a few actuation peaks or failed completely. The specimens placed in the hot/humid (climate-conditioned) environment failed after a few hours of actuation after 8 weeks of storage. These results clearly demonstrate that an additional coating for actuators used in wet or hot/humid environments is necessary for successful operation. To address these problems, appropriate coatings such as polymer, metal (in particular, gold), and ceramic coatings are currently being investigated and developed to withstand the water environment during experiments in a water tunnel.

5. Outlook and future tasks

The lessons learned from the current design work in water-tunnel experiments in active high-lift flows lead to further experimental and numerical research. One aim is the more detailed analysis of the closed-loop approach. With the reduced-order models derived from the experimental data, more sophisticated model-based controller laws such as H_∞ controllers will be incorporated. Further potential may be seen in the use of 3D actuation by varying the blowing ratio in a span-wise direction.

With a deeper understanding of unsteady actuation and improved controllers, the final step will be the setup of an experiment in a wind tunnel. With larger free-stream velocities, this leads to new requirements for the sensors and actuators.

Regarding the sensors, a hybrid combination of hot-film and pressure-sensing modules will be developed. This should increase the spatial resolution and could help in an understanding of the complex processes in the flow. Additionally, flexible hot-film sensors based on polyimide substrate could be embedded on the Coanda flap to measure the condition of flow downstream of the actuated lip.

The next steps interms of the actuated slot lip is to improve and qualify it for a water environment by the means of further investigation of diffusion processes, the long-term influence of humidity on electronic parts, and an appropriate insulation (coating). Further steps require the development of a control system for later water-tunnel operations in order to control each span-wise digit of the segmented slot lip separately. This will lead to an actuated slot lip with a length of 1 m built up of segments.

Besides further refinement of the current concept for experiments in a water tunnel, emphasis is also placed on the possible integration of this sensor-actuator system into a composite laminate for later composite applications in air environment at a larger scale.

Acknowledgements

This work was funded by the German Research Foundation in the framework of the Collaborative Research Center 880 ‘Fundamentals of High Lift for Future Civil Aircraft’. One of the authors (SB) gratefully acknowledges the financial support of the Volkswagen Foundation.

References

[1] Werner-Spatz C 2010 Flugzeuggesamtentwurf mit zirkulationskontrolle am hochauftriebssystem *CFF Forschungsbericht* 2010-02

[2] Liu Y 2007 Numerical simulations of the aerodynamic characteristics of circulation control wing sections *PhD Dissertation* School of Aerospace Engineering, Georgia Institute of Technology, Atlanta, GA

[3] Jones G S and Englar R J Advances in pneumatic-controlled high-lift systems through pulsed blowing *21st AIAA Applied Aerodynamics Conf. (Orlando)* AIAA 2003-3411

[4] Noack B R, Afanasiev K, Morzynski M, Tadmor G and Thiele F 2003 A hierarchy of low-dimensional models for the transient and post-transient cylinder wake *J. Fluid Mech.* **497** 335–63

[5] Ravindran S S 2006 Reduced order controllers for control of flow past an airfoil *Int. J. Numer. Methods Fluids* **50** 531–54
[6] Luchtenburg D M, Günther B, Noack B R, King R and Tadmor G 2009 A generalized mean-field model of the natural and high-frequency actuated flow around a high-lift configuration *J. Fluid Mech.* **623** 283–316
[7] Cohen K, Siegel S, McLaughlin T and Gillies E 2003 Feedback control of a cylinder wake low-dimensional model *AIAA J.* **41** 1389–91
[8] Pastoor M, Henning L, Noack B R, King R and Tadmor G 2008 Feedback shear layer control for bluff body drag reduction *J. Fluid Mech.* **608** 161–96
[9] Keller D and Rudnik R 2013 Aerodynamic aspects of the longitudinal motion of a high-lift aircraft configuration with circulation control, SFB880-fundamentals of high-lift for future commercial aircraft *CFF-Forschungsbericht* 2013-03 pp 147–58
[10] Burnazzi M and Radespiel R 2013 Design of a droopnose configuration for a coanda flap application *Proc. 51st AIAA Aerospace Sciences Meeting (Grapevine, TX)* AIAA-2013-0487
[11] 2012 PICMA® Stack Multilayer Piezo Actuators—P-882–P-888 *Technical Datasheet* (Lindenstrasse: PI Ceramic)
[12] Beutel T, Leester-Schädel M, Wierach P, Sinapius M and Büttgenbach S 2010 Novel pressure sensor for aerospace purposes *Sensors Trans. J.* **115** 11–9
[13] Schwerter M, Beutel T, Leester-Schädel M, Büttgenbach S and Dietzel A 2014 Flexible hot-film anemometer arrays on curved structures for active flow control on airplane wings *J. Microsyst. Technol.* **20** 821–9
[14] Wierach P 2006 Low profile piezo actuators based on multilayer technology *17th Int. Conf. on Adaptive Structures and Technologies (Taipei)* pp 274–84
[15] Gad-El-Hak M (ed) 2001 *MEMS Handbook* (Boca Raton, FL: CRC Press)
[16] Behr C 2013 *Entwurf Und Characterisierung Einer Aktuierten Ausblaslippe Für Ein Wasserkanalmodell Einer Tragflügelhinterkante* (Braunschweig: Diplomarbeit, Institute of Adaptronics and Funktional Integration, Technische Universität Braunschweig)
[17] Jensch C, Pfingsten K C and Radespiel R 2010 Numerical investigation of leading edge blowing and optimization of the slot and flap geometry for a circulation control airfoil *Notes on Numerical Fluid Mechanics and Multidisciplinary Design* vol 112 (Berlin: Springer)
[18] Jensch C, Pfingsten K C, Radespiel R, Schuermann M, Haupt M and Bauss S 2009 Design aspects of a gapless high-lift system with active blowing *Proc. DLRK 2009 (Aachen)*
[19] Pfingsten K C and Radespiel R Experimental and numerical investigation of a circulation control airfoil *47th AIAA Aerospace Sciences Meeting (Orlando)* AIAA 2009-533
[20] Pfingsten K C, Cecora R D and Radespiel R 2009 An experimental investigation of a gapless high-lift system using circulation control *Katenet II Conf. (Bremen)*
[21] Wild J Experimental investigation of mach- and reynolds-number dependencies of the stall behaviour of 2-element and 3-element high-lift wing sections *50th AIAA Aerospace Sciences Meeting (Nashville, TN)* AIAA 2012-108